

## CHAPTER 5:

### UPD OF COPPER ON AU(111)

The underpotential deposition of Cu on the low index faces of Au appears to be the most extensively studied system of underpotentially deposited (UPD) metals. It is certainly one of the few systems to be studied using both in situ and ex situ methods. Much has been said about copper deposition on Au(111) <sup>[40, 43, 47, 77, 82, 116-119]</sup>, which to date is still inarguably one of the most popular model systems for those interested in the basics of metal deposition.

It is difficult to calculate theoretically the UPD shifts <sup>[120]</sup> of copper ions using electrolytes containing different anions. One has to distinguish surface and solution effects. At one hand the anions stabilize the copper adatom/anion layers on Au(111). However, on the other hand some anions stabilize monovalent  $\text{Cu}^+$  ions, which may be taken as a solution effect. For example, the  $\text{Cu}^{2+}/\text{Cu}^0$  couple has a redox potential of 0.34 V vs. NHE, the redox potential for the  $\text{Cu}^{2+}/\text{Cu}^+$  couple for Br-containing electrolyte shifts from 0.16 to 0.65 V and to 0.56 V for chloride-containing electrolyte <sup>[121]</sup>.

#### 5.1 Influence of Anions

There exists a profound influence of the anions on the underpotential deposition of Cu on Au(111). First evidence was extracted by traditional electrochemical measurements such as cyclic voltammetry curves <sup>[68, 120]</sup>. More recently these ideas were confirmed by direct structural information, either from ex-situ experiments, e.g. by electron diffraction <sup>[122, 123]</sup>, or from in-situ structural probes such as STM <sup>[42, 47, 79]</sup>, AFM <sup>[117]</sup> and XRD <sup>[124]</sup>.

A three-step experiment was performed by Shi and Lipkowski <sup>[125, 126]</sup> to clarify the roles of the different adsorbates. With 0.1 M perchloric acid ( $\text{HClO}_4$ ) as the only electrolyte (i.e., with

no copper added), the CV current in the double layer range was weak, indicating that the ions present in the solution did not adsorb significantly on the surface. In the next step,  $K_2SO_4$  was added, introducing  $HSO_4^-$  and  $SO_4^{2-}$  ions into the solution. An adsorption peak then appeared, particularly during the positive-going scan. Radiochemical studies<sup>[49]</sup> indicate that this peak is due to sulfate adsorption with a maximum coverage of approximately 0.2 monolayers ML. This result agrees with chronocoulometric results<sup>[49]</sup> and with earlier STM studies<sup>[39, 79]</sup> in which a  $(\sqrt{3} \times \sqrt{7})$  sulphate adlayer was indicated on the positive side of the voltammetric peak in the absence of copper, without<sup>[79]</sup> or with<sup>[39]</sup> a perchloric-acid supporting electrolyte. Finally, addition of  $Cu^{2+}$  (as  $Cu(ClO_4)_2$ ) caused the appearance of two sharp current peaks which totally dominate the voltammogram, as also illustrated by our own data in Fig. 5.1. There is no two-peak feature in the CV if no copper is added. Evidently, the coadsorption of Cu and sulfate is mutually enhancing.

The deposition of copper on Au(111) and Au(100) surfaces was also theoretically investigated from a density functional point of view<sup>[127]</sup>. The analysis of the different energetic contributions to the so-called underpotential shift indicates that the deposition of Cu on any of these surfaces should occur at overpotentials. Therefore, some other factors must be taken into account to explain the experimental results. One of them is the anion coadsorption. The covering of Au(111) and Au(100) single crystal surfaces by a Cu(1x1) adsorbed monolayer should be accompanied by a strong change in the work function of the system, of the order of 1 eV<sup>[127]</sup>. This fact should play a very important role in promoting anion coadsorption due to the concomitant shift of the potential of zero charge of the system.

It was soon realized, however, that strongly adsorbing anions, in particular the specifically adsorbing halide anions chloride, bromide and iodide, can modify the metal adsorption behavior even when present only at small concentrations<sup>[76, 120, 128]</sup>. Such effects have been observed, e.g., for Cu-UPD on Pt(111) in perchlorate and fluoride solution, where the addition of  $10^{-6}$  to  $10^{-4}$  M HCl causes drastic changes in the shape of the current potential curves<sup>[128]</sup>. It was found that the  $(\sqrt{3} \times \sqrt{3}) R30^\circ$  structure unanimously reported for the Cu adlayer in  $H_2SO_4$  solution is changed into a long-range modulated hexagonal structure in the presence of trace amounts of  $Cl^-$  in the electrolyte<sup>[41, 42, 47]</sup>. These effects should become even more drastic in the electrolytes with weakly or non-specifically adsorbing anions such as the perchlorate anion. Chloride as well as

bromide is found to form adsorbed bilayers with the copper, the former being adsorbed on top of the UPD layer<sup>[129]</sup>.

The other remarkable feature is the anion influence on the deposition kinetics of Cu. The deposition of copper is extremely slow in perchlorate solution, where formation of a full monolayer will require as much as half an hour.

## 5.2 In Sulfuric Acid Media

The deposition of the first Cu monolayer on Au(111) at underpotentials in sulfuric acid electrolyte has been studied in great detail both by *in situ* techniques like CV<sup>[42, 125, 126, 130-133]</sup> chronocoulometry<sup>[42, 48, 80, 126, 131, 134-137]</sup>, STM<sup>[41-43, 47, 122]</sup>, AFM<sup>[46, 117]</sup>, FTIR<sup>[138]</sup>, x-ray-absorption spectroscopy (EXAFS and XANES)<sup>[37, 118]</sup>, surface x-ray scattering<sup>[40, 124]</sup>, QCM<sup>[40, 134]</sup>, and by *ex situ* techniques, such as LEED, RHEED and AES<sup>[139-142]</sup>.

The cyclic voltammogram of Au(111) in 1 mM Cu(ClO<sub>4</sub>)<sub>2</sub>, 0.100 M HClO<sub>4</sub> and 0.020 M Na<sub>2</sub>SO<sub>4</sub> electrolyte is demonstrated in Fig. 5.1. Two well-defined and sharp peak pairs correspond to two energetically separated redox steps, which is clearly discernible in the voltammogram. Considering the electrochemical results, one would expect, a priori, that two different copper ad-structures would be present. After the first deposition peak (A), an intermediate copper layer (ca.  $\Theta = 2/3$ ) coadsorbed with sulfate ions, and in the second step (peak B), a full monolayer of copper (1x1) on gold is formed. The small shoulder (C) at the second deposition peak is the result of two different nucleation processes, one taking place on surface defects and the other on well-ordered (111) terraces;<sup>[143]</sup> thus, the dependence on the surface quality of the electrode is evident.

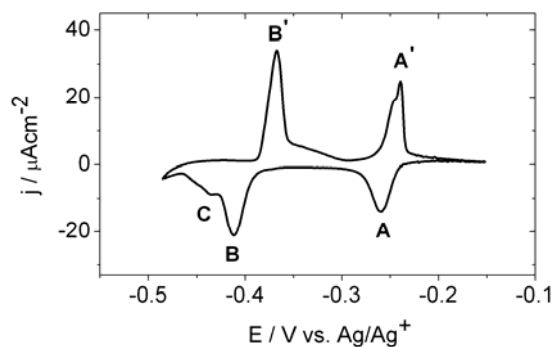


**Figure 5.1:** The cyclic voltammogram of 1 mM  $\text{CuSO}_4$  + 0.1 M  $\text{HClO}_4$  + 0.020 M  $\text{Na}_2\text{SO}_4$  on Au(111). Sweep rate: 5 mV/s.

In the literature two different coulometry results have been reported for the copper underpotential process on Au(111) in the entire UPD region: one is around  $460 \mu\text{Ccm}^{-2}$  [42, 134, 136] and another is around  $350 \mu\text{Ccm}^{-2}$  [48, 126, 131, 137]. The theoretical value (based on the surface atom density) necessary for the deposition of a fully discharged monolayer of copper ( $\text{Cu}^{2+} \longrightarrow \text{Cu}^0$ ) would be  $440 \mu\text{Ccm}^{-2}$ . According to Refs. [48, 126], the variation of the sulfate concentration from 0.01 mM to 5 mM changes the total charge transfer only by about 5% at the negative end of the UPD potential range. Likewise, the variation of the  $\text{Cu}(\text{ClO}_4)_2$  concentration from 0.01 mM to 5 mM also did not yield significant changes in the total charge. Thus, it is highly unlikely that the large discrepancies between the experimentally measured charge transfers are due to the differences between the used electrolyte compositions. Rather, the difference is likely the result of different measurement criteria, since in arriving at the value of  $350 \mu\text{Ccm}^{-2}$ , a charge of zero was assigned for the potential in the middle of the first peak (A) [82] due to the coadsorption of sulphate anion with copper. The addition of the charge that would correspond to the half of the first peak would give a charge value that is close to  $440 \mu\text{Ccm}^{-2}$ . Secondly, the large charge transfers observed in Refs. [42, 136] were likely due to unexpectedly large roughness of the electrodes.

The first structure determination of the Cu adlayers were done in UHV by Kolb and co-workers [144]. RHEED and LEED revealed two different structures that were interpreted as a  $(\sqrt{3} \times \sqrt{3}) \text{R}30^\circ$  honeycomb structure with  $\Theta_{\text{Cu}} = 0.67$  after the first deposition peak. Another was investigated as a (1x1) structure,  $\Theta_{\text{Cu}} = 1$ , after the second deposition peak. AES measurements also indicated that (bi)sulfate adsorption on the Cu adlayers was stronger than that on the bare Au(111) electrode. This results agree with the radiotracer [45, 145] and FTIR [138] measurements of Cu UPD on polyoriented gold.

The second peak corresponds to filling the  $(\sqrt{3} \times \sqrt{3}) \text{R}30^\circ$  structure to form a commensurate (1x1) monolayer. *In situ* EXAFS data for Au(111)/Cu are fully consistent with the picture assembled by Kolb and coworkers. Blum et. al. [146] attributed to coordination of (bi)sulfate anion onto the Cu UPD layer at low underpotentials.

In some papers<sup>[130, 147, 148]</sup> the formation of  $\text{Cu}^+$  as an intermediate during the deposition of copper on gold electrode was stated as a possibility only in the OPD region. However, Omar et al.<sup>[131]</sup> claimed that a partial discharge of  $\text{Cu}^{2+}$  to  $\text{Cu}^+$  does occur in the UPD region and that the strong repulsive interaction between the monovalent adatoms is compensated by simultaneous coadsorption of sulfate ions. Additionally, they discarded the possibility of formation of  $\text{Cu}^+$  by the disproportionation as a predominant reaction. Shi and Lipkowski<sup>[125]</sup> claimed that the oxidation state +1 is the result of polar character of the chemisorption bond rather than a result of the formation of an intermediate in a stepwise redox reaction.

On the basis of what is already known from the above overview, it is our aim to answer some of the open questions and to contribute some new findings with respect to the UPD process of copper on Au(111) in the presence of sulphate anion.

## **5.2.1 Chronocoulometry experiments**

### **5.2.1.a Set-I**

To estimate kinetic the parameters of the copper deposition on the Au(111) electrode in the sulfate anion containing electrolyte, a set of potentiostatic current transients have been measured by us applying the following routine:

- i) Scanning from 0.2 V to the second formation peak potential (peak B, -0.41 V) with a scan rate of 5 mV/s and waiting there for different times.
- ii) Jumping back from the formation potential to the potential where no deposition occurs (-0.2 V).

### **Formation**

During the waiting time at the formation potential (peak B) the current-time evolution presented in Fig. 5.2 a,b occurred. It can be recognized that the almost zero current is reached after one minute; afterwards, no change is observed at further time scale. The formation process does not obey the nucleation and growth law due to the lack of well-defined minimum-maximum peak. Rather, it might be a diffusion controlled process due to exponentially decaying of current density with time.

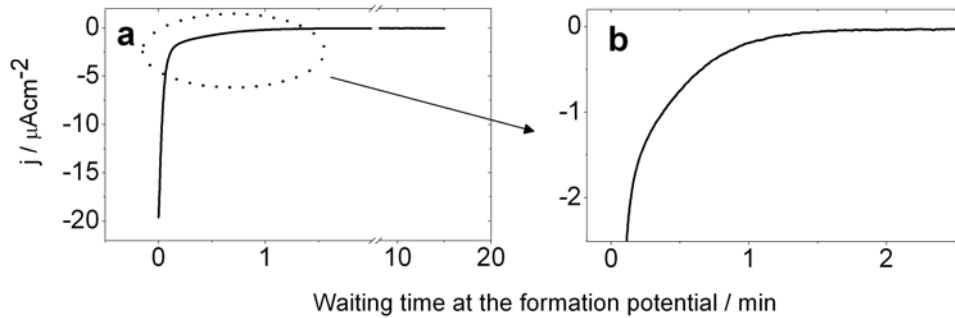


**Figure 5.2 a)** Current-time transient measured at the formation potential B,  $-0.41$  V, zoomed in b.

### Dissolution

The dissolution transients shown in Fig. 5.3 imply two different dissolution states. The first one takes place at early milliseconds (0-100 ms) including double layer charging exhibiting an exponentially decaying process. The dissolution transient in this time scale gets broader and reaches a steady state if we wait more than 1 minute at the formation potential.

The second state in dissolution is observed at further milliseconds (100-400 ms) exhibiting a smoother current maximum. The current maximum shifts to longer time after waiting just one minute and the shape and the peak position of the transients do not change with further waiting times. In addition, the shape of the transients implies that the dissolution of Cu layer obeys a “hole” nucleation and growth law.

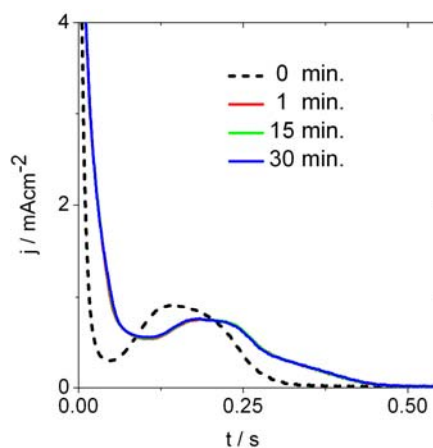


**Figure 5.3:** Dissolution transients obtained after waiting different times at peak B and stepping into dissolution potential region.

### Charge density diagram

The integration of dissolution transients results in the charge-potential diagram shown in Fig. 5.4 waiting at peak B. The limiting value of the consumed charge ( $325 \pm 5 \mu\text{Ccm}^{-2}$ ) is reached after waiting two minutes. This value is almost  $100 \mu\text{Ccm}^{-2}$  lower than the theoretical one.

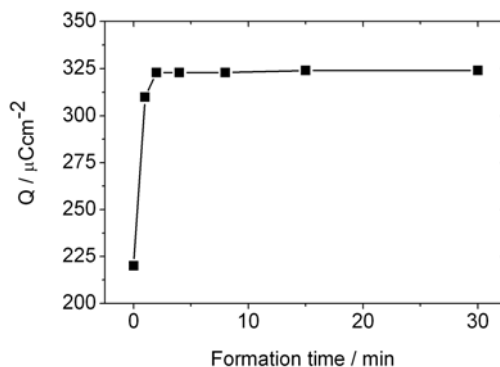


**Figure 5.4:** Charge values obtained after the integration of the dissolution transients.

#### 5.2.1.b Set-II

As an addition to the above potential-step experiments, three different potential steps were applied as stated in the following routines (Fig. 5.5):

A: scanning from 0.1 V with the scan rate of 5 mV/s to -0.485 V, then step into -0.2 V.

B: scanning from 0.1 V with the scan rate of 5 mV/s to -0.485 V, then step into -0.3 V.

C: scanning from 0.1 V with the scan rate of 5 mV/s to -0.350 V, then step into -0.2 V.

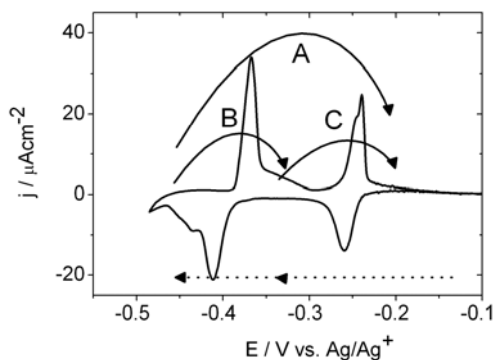


**Figure 5.5:** The cyclic voltammogram on which the coulometric measurements are based in the electrolyte of 1 mM  $\text{CuSO}_4$  + 0.1 M  $\text{HClO}_4$  + 0.020 M  $\text{Na}_2\text{SO}_4$  with the sweep rate 5 mV/s. The arrows show the routines of the potential-step experiments.

The dissolution transients and the charge density values under these curves are presented in Fig. 5.6. In routine A, two well defined dissolution processes related with the deposition (dissolution) of Cu in two steps shown in the CV (Fig. 5.6) take place. At early milliseconds (0-75 ms), as well double layer charging as the dissolution of the Cu adatoms, deposited at the second step of voltammogram, takes place. At further milliseconds (100-400 ms), dissolution of the Cu adatoms deposited at the first step (honeycomb structure) takes place. The charge density consumed in the entire UPD corresponds to  $337 \pm 7 \mu\text{Ccm}^{-2}$ .

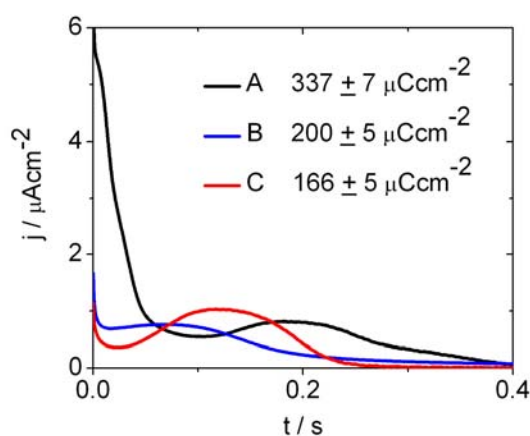


**Figure 5.6:** Dissolution transients obtained as result of the routines (the rectangular shapes sign the analysed regions for Avrami study) (a) and the corresponding changes of Avrami slopes (stars points the slopes of linear fit of entire Avrami curve) (b).

At the other two transients, B, C, dissolution process proceeds at only one step in addition to the small capacitive contribution at the beginning. The charge densities for B and C are  $200 \pm 5 \mu\text{Ccm}^{-2}$  and  $166 \pm 5 \mu\text{Ccm}^{-2}$ , respectively. The peak position of the transient C locates at longer times compared to that of B. It reveals that the adlayer formed in C [ $(\sqrt{3} \times \sqrt{3})\text{R}30^\circ$ ] is stronger than the (1x1) adlayer formed in B. Therefore, the contribution of sulphate (bisulphate) anion to the strength of honeycomb structure is obviously seen.

Considering the charge values obtained from our transients, they are inconsistent with the authors claiming  $460 \mu\text{Ccm}^{-2}$  for full coverage [42, 134, 136], however, consistent with the values obtained by Lipkowski and some other authors [48, 126, 131, 137] claiming  $350 \mu\text{Ccm}^{-2}$ . It is commonly proved from STM [41, 43, 47], AFM [46, 117], LEED [144] techniques that  $(\sqrt{3} \times \sqrt{3})\text{R}30^\circ$



honeycomb structure with  $\Theta_{\text{Cu}} = 0.67$  is formed after the first deposition peak. From our coulometric results, without considering the sulphate coadsorption it can be proposed that Cu is approximately +1 oxidation state after the first deposition peak, because the consumed charge in transient C, (Fig. 5.6), is  $166 \pm 5 \mu\text{Ccm}^{-2}$  corresponding closely to 2/3 surface coverage ( $\Theta_{\text{Cu}} = 0.67$ ). However, if we consider coadsorption of (bi)sulphate anion leading some charge contribution as also claimed by Herrero et.al. [82], the oxidation state of copper adatoms must be close to 0. We expect that the degree of the transfer is about  $80 \pm 10 \mu\text{Ccm}^{-2}$  (half charge of first deposition peak [82]). In order to achieve the charge of  $300 \mu\text{Ccm}^{-2}$ , which corresponds to 2/3 coverage ( $\text{Cu}^0$ ), the deficit is around  $50 \pm 10 \mu\text{Ccm}^{-2}$ . It means that copper ion is not totally reduced to zero, may be between 0 and +0.5.

### 5.3 In Perchloric Acid Media

In this section, we focus on the underpotential deposition behavior of Cu in perchloric acid electrolyte on Au(111) electrode, which was studied quantitatively by cyclic voltammetry, chronocoulometry and XPS techniques. It will be compared with the deposition of copper in sulfuric acid.

Perchlorate was often considered to be an inert anion which does not adsorb on Au electrode or at least its adsorption was treated as sufficiently weak to be neglected. However, some authors found that the  $\text{ClO}_4^-$  anion adsorbs on Au(111) weakly in comparison with  $\text{SO}_4^{2-}$  ( $\text{HSO}_4^-$ ) or  $\text{Cl}^-$  [36, 149]. When present in excess,  $\text{ClO}_4^-$  anions can even compete for the adsorption sites on Au(111) with  $\text{HSO}_4^-$  [149]. In solutions containing only  $\text{ClO}_4^-$  anions, there is a strong kinetic hindrance of Cu deposition [34]. This is clearly observed by cyclic voltammetry (Fig. 5.7.a) where a single, sharp anodic desorption peak of Cu from Au(111) is contrasted by only a small and broad deposition peak indicating the kinetic hindrance. The presence of even the traces of  $\text{Cl}^-$  anions greatly enhances the kinetics of Cu UPD process on Au(111). Some authors claim this evidence presented in the literature as an evidence of the specific adsorption of  $\text{ClO}_4^-$  is probably better interpreted as having been caused by impurities of  $\text{Cl}^-$  [77].

To compare our results with those of other authors and to verify our experimental system, a cyclic voltammogram for 1 mM  $\text{Cu}(\text{ClO}_4)_2$  in 0.1 M  $\text{HClO}_4$  was recorded with a scan rate of 5 mV/s (Fig. 5.7.a, solid line). The picture involves the deposition of copper in sulfate containing

electrolyte (dashed line). These results are in agreement with those previously reported ones<sup>[34]</sup>. The sharp anodic peak observed only in perchlorate containing electrolyte around -0.27 V corresponds to the Cu desorption. From the small and broad cathodic peaks, it is clear that the Cu deposition process is kinetically hindered in the presence of the perchlorate anion. This behavior is similar to that observed in the case of Cd UPD on Au(111) in ultrapure HClO<sub>4</sub> aqueous solutions<sup>[150]</sup>. The authors<sup>[150]</sup> explained in a way that cadmium ion upon adsorption retains part of its original charge. This causes a slow deposition kinetics induced by hindrances in the surface nucleation due to repulsive interactions between the charged adsorbates. This effect can be offset by the addition of anions (i.e., SO<sub>4</sub><sup>2-</sup>) in the solution which can coadsorb on the surface and promote the formation of nuclei by screening the charge.

In Fig. 5.7.b the potential region is shown in which normally bulk deposition is observed in sulfate containing electrolyte. In perchlorate electrolyte, UPD as well as the bulk deposition of copper are kinetically hindered. Even in scans to more negative potentials (-0.8 V) with 5 mV/s rate, only a small bulk stripping peak around -0.38 V is observed. The charge values corresponding to stripping peaks for UPD and OPD potential regions are  $100 \pm 10$  and  $240 \pm 10$   $\mu\text{C}/\text{cm}^2$ , respectively. The formation of a fully discharged copper monolayer ( $\text{Cu}^{2+} \longrightarrow \text{Cu}^0$ ) would consume 440  $\mu\text{C}/\text{cm}^2$ . The charge value consumed in bulk potential region corresponds to almost a half monolayer of fully discharged copper. This result will be discussed with the next coulometry results.

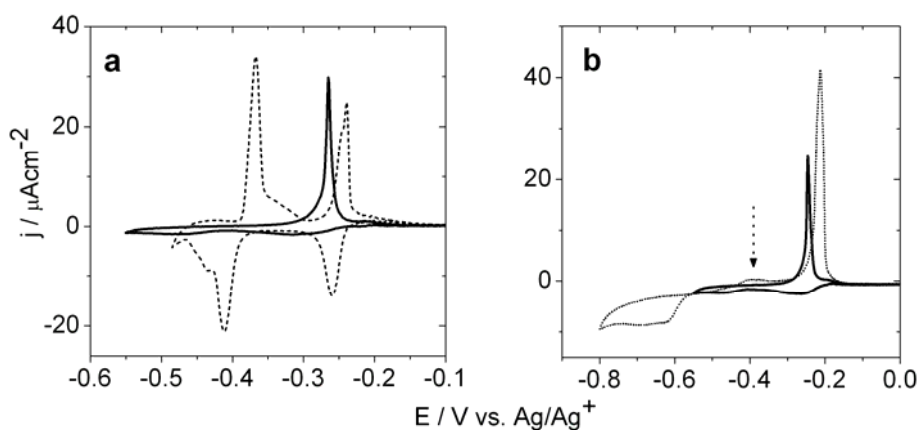


**Figure 5.7:** The cyclic voltammograms **a:** 1 mM Cu(ClO<sub>4</sub>)<sub>2</sub> + 0.1 M HClO<sub>4</sub> + 0.060 M NaClO<sub>4</sub> (solid) and 1 mM CuSO<sub>4</sub> + 0.1 M HClO<sub>4</sub> + 0.020 M Na<sub>2</sub>SO<sub>4</sub> (dash) on Au(111). **b:** Scanning to bulk potential region in perchlorate electrolyte. Sweep rates: 5 mV/s.

It is worth noting that the voltammogram of Cu UPD scanned at 1 mV/s rate in perchlorate containing electrolyte has a positive current peak during cathodic scan (Fig.5.8). This kind of behaviour was also observed in sulphate containing electrolyte [82]. Therefore, This feature might indicate that perchlorate is coadsorbed with copper ion and some degree of charge transfer from perchlorate takes place.

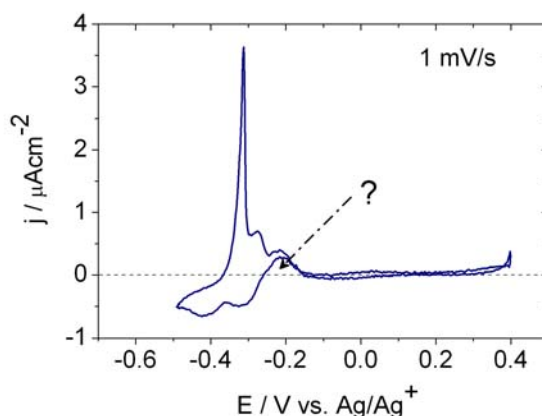


**Figure 5.8:** The cyclic voltammogram of 1 mM  $\text{Cu}(\text{ClO}_4)_2$  + 0.1 M  $\text{HClO}_4$  + 0.060 M  $\text{NaClO}_4$ .

### 5.3.1 Acidity Dependence

The relationship between the metal deposition and the pH of the electrolytic bath is an important issue to be determined. Since during the UPD/OPD process, the electrode surface (top outmost layer) is covered by different materials, its reactivity with solution anions could be altered significantly by changes in pH. It is known that small amounts of specifically adsorbed anions accelerate the charge transfer, due to local electrostatic effects in the electric double layer and the process of metals electrodeposition in general [82, 151]. Copper oxides ( $\text{Cu}_x\text{O}$  or mixed oxides  $\text{Me}_x\text{Cu}_y\text{O}$ ) formed by a slow surface reaction between coadsorbed oxygen compounds and copper adatoms act as the active centers for Cu adlayer formation and subsequent overpotential deposition (OPD) [151].

C. Meyer, a member of our group, investigated the copper deposition in sulfuric acid media depending on the pH changes. He observed that the increase in pH from 1.24 to 4.56 of solutions leads to noticeable changes in the CV profile. The changes in CVs profiles correspond to a positive shifting at the UPD peaks (40 mV and 75 mV for the first and second ones, respectively). Bulk deposition was also accelerated upon increasing pH [109].

Kolb and coauthors<sup>[152]</sup> studied the deposition of copper on Au(111) in sulfate solutions with pH varied from 2 to 4. They observed significant changes in the shape of the current transients, indicating different copper deposition mechanisms at different pH values. Transients with a well-defined current maximum observed at pH 4 were associated with a 3D progressive electrocrystallization. At pH 2, the nucleation changed from a 3D progressive to a 3D instantaneous process. The change in nucleation mechanism is caused by a decrease in nucleation sites at the electrode surface. Because sulfate (pH>2) becomes bisulfate at pH<2. Strongly adsorbed bisulfate supposedly hinders the Cu nucleation sites<sup>[152]</sup>. At pH 1, when the copper deposit is presumably covered by bisulfate, copper nucleation and growth during OPD proceed much more slowly, but on a greater number of active sites. At pH 4 for copper surfaces covered by sulfate, fewer active sites, but a faster nucleation rates were found. This allows the conclusion that sulfate adsorbs more strongly than bisulfate at the copper deposit and blocks some of the deposition active sites<sup>[151]</sup>.

In our study, we have investigated the acidity dependence of Cu deposition on Au(111) in perchloric acid. The cyclic voltammograms in Fig. 5.9 illustrate deposition of copper on Au(111) in 0.1 M and 0.001 M HClO<sub>4</sub> solutions (unfortunately, the ionic strengths of electrolytes are not the same, but this does not lead a significant difference). Lowering the acidity does not influence the deposition of copper in UPD region significantly. However, it accelerates the Cu bulk deposition and dissolution (peaks A, B). At higher acidity of the electrolyte, even if we scan to bulk potential region (Nernst potential of Cu is -0.49 V vs. Ag/Ag<sup>+</sup>), bulk deposition of copper is not observed.

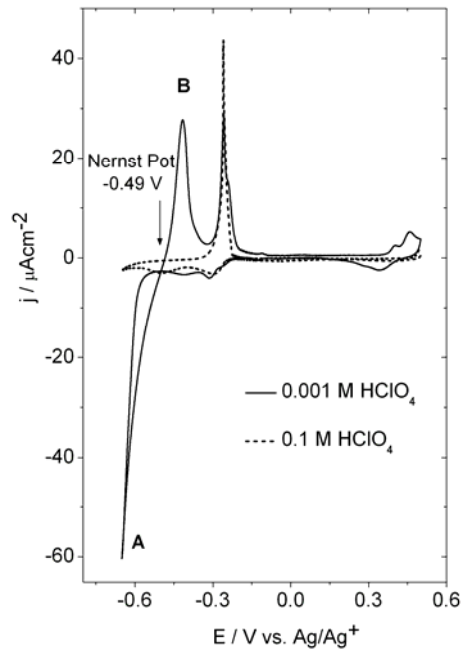


**Figure 5.9:** The cyclic voltammograms of  $1 \text{ mM Cu}(\text{ClO}_4)_2 + 0.06 \text{ M NaClO}_4 + \text{HClO}_4$ :  $0.1 \text{ M}$  (dot line),  $0.001 \text{ M}$  (solid line). Sweep rates:  $5 \text{ mV/s}$ .

The reason behind these changes is the increase of active species,  $\text{OH}^-$ . Hydroxide ions on a monolayer of copper adatoms and Cu crystallites provides an accelerated charge transfer (local electrostatic double layer effects of electronegative species) and probably increases the number of active centers for three-dimensional nucleation.

### 5.3.2 Chronocoulometric Studies

The following sequence of potential steps is identical with which was applied in  $\text{SO}_4^{2-}$  containing electrolyte. The current transients were obtained applying the following routine (Fig. 5.10) in the electrolyte containing  $1 \text{ mM Cu}(\text{ClO}_4)_2$ ,  $0.06 \text{ M NaClO}_4$ ,  $0.1 \text{ M HClO}_4$ :

- (Segment 1) Scanning from  $0.2 \text{ V}$  to the formation peak potentials (peak A:  $-0.31 \text{ V}$ , peak B:  $-0.44 \text{ V}$ ) with a scan rate of  $2 \text{ mV/s}$ ,
- (Segment 2) Waiting at the formation potentials for different times,
- (Segment 3) Stepping from the formation potentials to the potential where no deposition occurs ( $-0.15 \text{ V}$ ).

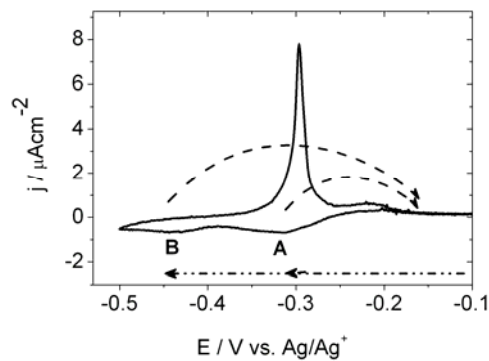


**Figure 5.10:** The cyclic voltammogram on which the coulometric measurements are based in the electrolyte of 1 mM  $\text{Cu}(\text{ClO}_4)_2$  + 0.1 M  $\text{HClO}_4$  + 0.060 M  $\text{NaClO}_4$  with the sweep rate 2 mV/s.

### 5.3.2.a Waiting at the formation potential A (-0.31 V) & Avrami analysis

#### Formation transient

The current density-time curve shown in Fig 5.11.a was obtained during waiting at the formation potential, -0.31 V (segment 2). In first minutes of the waiting period, the current density (as absolute value) decreases fast; afterwards it gradually approaches to zero current density. Application of Cottrell equation (Eq. 3.8) to the first minutes of the transient gives the curve shown in Fig. 5.11.b. The current density is almost linearly dependent to the reciprocal square root of time. It seems that the adsorption is a diffusion controlled process, however, considering the limitations of the equation the time necessary for this process must be lower than 0.2 seconds.

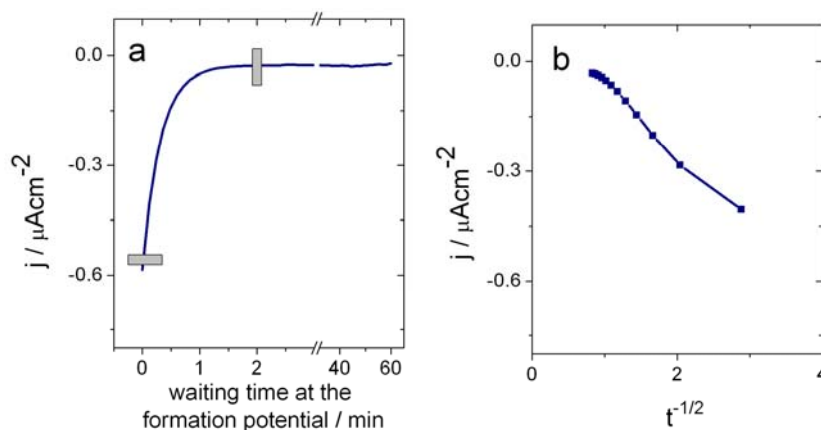


**Figure 5.11:** Current-time transient measured at the formation potential A (-0.31 V) (a) and the application of Cottrell equation to the initial region of the transient.

### ***Dissolution transient***

The shapes of the current transients obtained after jumping from  $-0.31$  V to  $+0.15$  V are shown in Fig. 5.12. They are typical minimum/maximum transients indicating that a nucleation and growth process takes place during desorption. The rate of the dissolution process is fast and depends not on the waiting time. Increasing waiting time the peak positions do not change significantly.

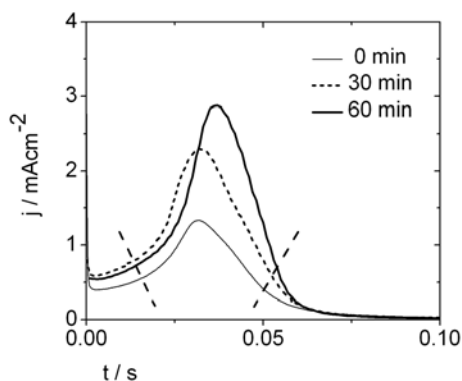


**Figure 5.12:** **a:** Dissolution transients obtained after waiting at the peak A ( $-0.31$  V) and stepping into the dissolution potential  $-0.15$  V. **b:** The corresponding changes of Avrami slopes. The dashed lines determine the range of Avrami analysis.

### ***Avrami analysis of the dissolution transients***

In order to get additional information about the dissolution process of Cu-UPD, the transients have been analysed using Avrami theorem. At a first glance to the shapes of the transients, we can state that the dissolution process obeys nucleation and growth mechanism. Because to the process for the present case is dissolution, we will call it as the “hole” nucleation and growth mechanism. As already mentioned before (section 2.5), the slopes of the Avrami curves are taken as a criterion to know the detailed mechanism of dissolution. Avrami plots show the relationship of  $\ln\ln[1/(1-\Theta)]$  versus  $\ln t$ .

For the analysed transients, we interpret the Avrami curves considering two different viewpoints;

- (i) the conventional point of view (see Table 2.1),
- (ii) the predator prey model

The procedure of Avrami analysis for our systems is as follows:

Firstly, the transients were integrated depending on the time. Secondly; surface coverage (condensed phase) values depending on the time were calculated considering  $350 \mu\text{Ccm}^{-2}$  as the maximum charge density for a full monolayer of copper. The data belonging to the initial and the final 5-10 % coverage depending on the shape of transient were removed. Afterwards, the calculation of “ $\ln\ln[1/(1-\Theta)]$ ” and “ $\ln t$ ” values was performed. The analysed parts of transients were marked with lines like in Fig. 5.12.

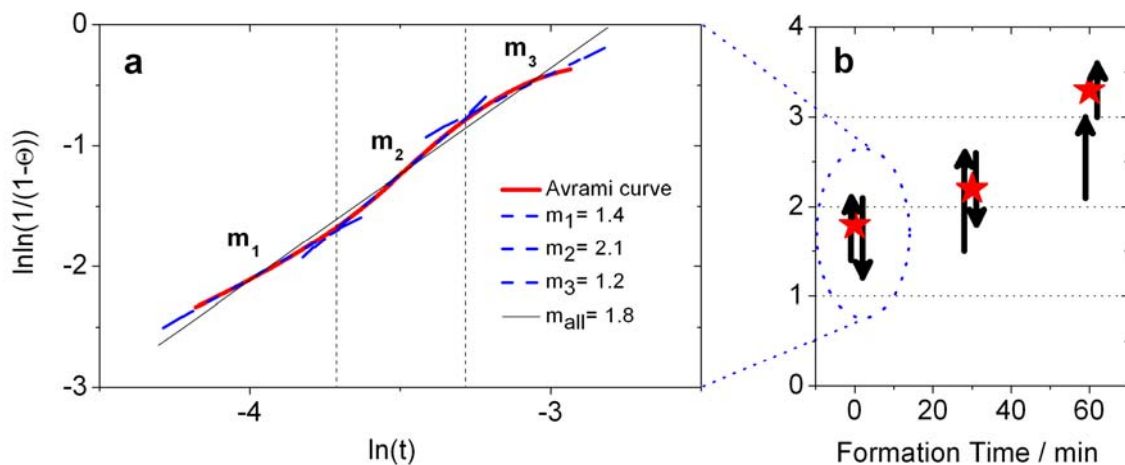


**Figure 5.13** a) The representative Avrami curve of the transient shown in Fig. 5.12 (without waiting). The Avrami curve is divided to three parts and each is fitted linearly. b) The arrows illustrate the change of Avrami slopes and the red stars point out the slopes of the fit curves of entire Avrami curves ( $m_{all}$ ).

In the present part, only one representative Avrami curve (Fig. 5.13.a, red curve) is shown as an example. This curve is obtained analysing the dissolution transient obtained without waiting (Fig. 5.12, thin curve).

It is obviously recognized that the Avrami plot is not strictly linear. The non-constant slope can be caused by a time dependent undersaturation during dissolution. We have generally divided a nonlinear Avrami curve into two or three main parts depending on the main changes in slope values. The straight arrows (Fig. 5.13.b) have been plotted to indicate the trends of the slopes. The red star as shown at the same representation points out the slope value for the fit



curve (thin-black line in Fig. 5.13.a) of entire considered part. This is important because in this way the weights of different slope values in one Avrami curve can be recognized. In the next pages, only this kind of representation will be used for Avrami analysis. The next dissolution transients are analysed in the same manner described above.

The following interpretation can be done for all analysis shown in Fig. 5.13.b. From the conventional point of view, Avrami curves corresponding to the transients waiting half an hour and without waiting at the formation potential exhibit similar results. Avrami slopes for those transients are around 2. This indicates that the instantaneous nucleation combined with constant growth or progressive nucleation with diffusion growth take place. The slope for the transient waiting one hour is slightly over 3 revealing the progressive nucleation combined with constant growth mechanism.

From the predator-prey point of view, Avrami slopes for the first two transients exhibit an increase followed by a decrease. The driving force in the present system is undersaturation. The lower the undersaturation is, the lower is the driving force for the dissolution and. Avrami slope increases with lower undersaturation and decreases with higher undersaturation. Having this interpretation in mind the following can be stated:

At the beginning part of both considered transients, Avrami slope is lower compared to the slope of the next part. It means that the dissolution of copper adatoms at the initial stage is faster in comparison to desorption. The reason for this result might be the edge and kink effect, which catalyzes the dissolution at the beginning. The higher Avrami slope value at the middle of the transients indicates that the rate of dissolution get slower and the copper adatoms adsorbed on terraces are desorbed. . The decrease in the slope value at the final part of dissolution most likely indicates that dissolution gets again faster in comparison to desorption. The decrease in the sizes of the islands might be the reason. This effect is similar to the increasing vapour pressure with smaller sizes of droplets as is well known from classical thermodynamics. We assume that the decreasing stabilization of the condensed phase (UPD) with decreasing size of the islands is the important factor for determining the overall kinetics.

Interestingly, for the last transient the slope continuously increases. It implies that the dissolution gets slower compared to beginning. The probable reason is the formation of the more ordered and stable UPD-layer as a result of longer waiting at the formation potential.

### Charge density diagram

The integration of the dissolution transients results in the charge-time diagram given in Fig. 5.14. The charge values were fit according to the exponential growth law shown with solid line. The hole formation in the copper layer is a very slow process and the consumed charge finally reaches to  $82 \pm 4 \mu\text{C}/\text{cm}^2$  at the end of one hour. By extrapolation of the fit function, one comes to  $85 \pm 4 \mu\text{C}/\text{cm}^2$  at the end of 3 hours.

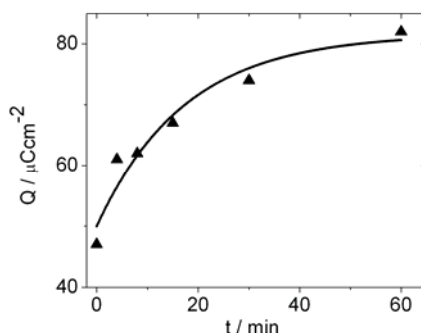


**Figure 5.14:** Charge density-formation time diagram obtained after the integration of the dissolution transients and the curve fitted according to the exponentially growth.

#### 5.3.2.b Waiting at the formation potential B (-0.44 V) & Avrami analysis

##### Formation transient

During the waiting time at the formation potential (peak B) the current-time evolution presented in Fig. 5.15 could be obtained. In this figure a well-defined minimum/maximum peak located at 12<sup>th</sup> minute is observed. This behavior of Cu UPD in perchlorate indicates the monolayer formation obeys the nucleation and growth law.

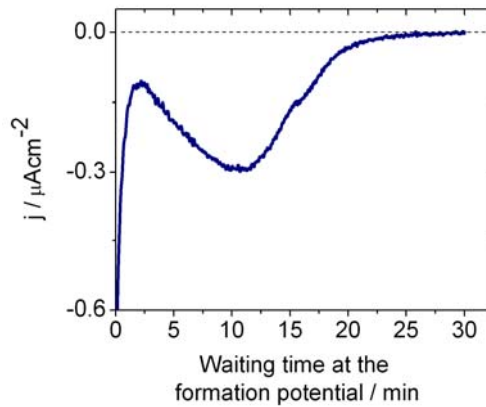


**Figure 5.15:** *a)* Current-time transient measured at the formation potential B (-0.44 V). *b)* The corresponding changes of Avrami slopes (star points the slope of the fit curve belonging to the entire Avrami plot).

### Dissolution transients

The shape of the dissolution transients shown in Fig 5.16 implies that the process obeys a *hole* nucleation and growth law. With further waiting, the dissolution peaks get broader and the time, needed for dissolution, shifts to longer times indicating the formation of ordered and stable copper monolayer. Compared to the first condition (waiting at the peak potential A, -0.31 V), the dissolution is slow. It indicates that the copper adlayer has a more metallic character.

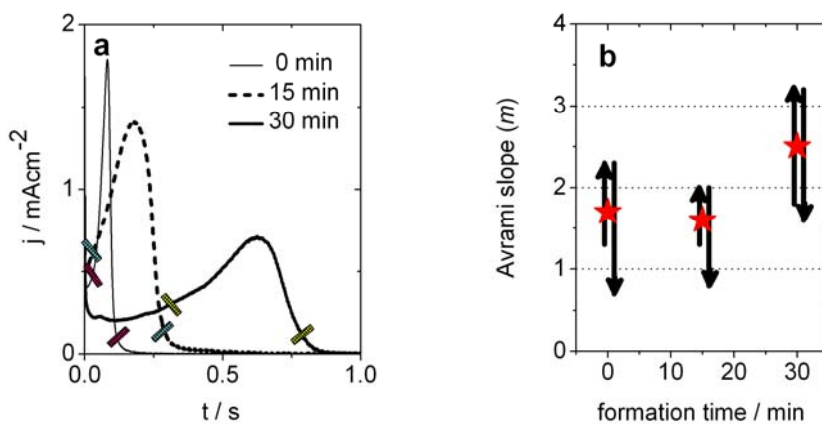


**Figure 5.16:** Dissolution transients obtained after waiting at the peak B (-0.44 V) and stepping to dissolution potential region. **b):** The corresponding changes of Avrami slopes depending on waiting time slopes (stars point the slopes of the fit curves belonging to the entire Avrami plot).

The Avrami curves were obtained analyzing the restricted parts of the transients (signed with rectangular shapes in Fig. 5.16.a). The changes in the slope values are illustrated in Fig.5.16.b. As different from the former Avrami results, in the present case slope values span much larger values. The first two dissolution transients are similar each other. The slope values at the beginning are around 1 indicating the presence of instantaneous nucleation combined with surface diffusion growth mechanism. At further stages of dissolutions the slope values climb to 2 revealing the progressive type nucleation with surface diffusion mechanisms or instantaneous nucleation combined with constant growth. The slope of the Avrami curve belonging to the third transient (waiting 30 min) varies between 2 and 3. It means that at the first and the last stages of the transient, the mechanism is either instantaneous nucleation with surface diffusion constant growth or progressive nucleation with surface diffusion. However, at the middle stage, it is progressive nucleation with constant growth.

All transients exhibit similar behaviour (increase-decrease) about the change of Avrami slope. It indicates that the dissolution of copper adatoms is slow at the middle stage of transients compared to the initial and final stages. The possible reason is explained in Section 5.2.1.a.

### ***Charge density digram***

The integration of dissolution current transients gives the charge-potential diagram shown in Fig. 5.17. The consumed charge increases exponentially and reaches  $305 \pm 5 \mu\text{C}/\text{cm}^2$  within half an hour. It seems that even after 30 minutes waiting time; the surface is not covered by a fully discharged copper monolayer.

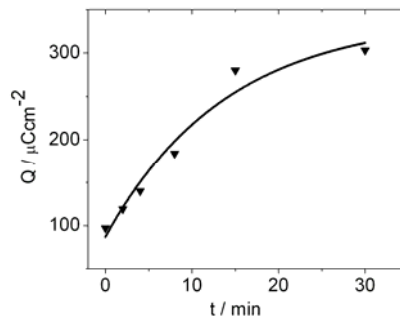


**Figure 5.17:** Charge density-formation time diagram obtained after the integration of the dissolution transients and the curve fitted according to the exponentially growth.

### ***Monitoring the CV after waiting***

The change depending on the waiting time at peak B was also monitored in CV shown in Fig. 5.18. The solid curve is the first cycle without adjusting anywhere and it has mainly one stripping peak. Whereas, after waiting half an hour at -0.440 V at the second cycle, the main stripping peak with two shoulders is observed (dashed curve). It reveals that the adlayer has at least three different overlapping adsorption states. The calculated areas under these peaks are  $70 \pm 10 \mu\text{Ccm}^{-2}$  and  $270 \pm 10 \mu\text{Ccm}^{-2}$  which are close to the values calculated from coulometry above.

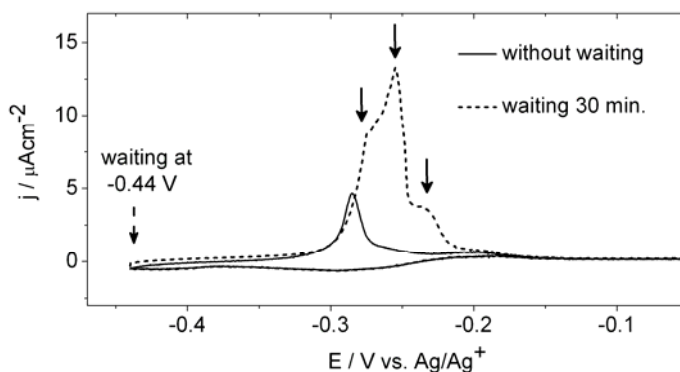


**Figure 5.18:** The cyclic voltammograms of 1 mM  $\text{CuClO}_4$ , 0.1 M  $\text{HClO}_4$  + 0.060 M  $\text{NaClO}_4$  on Au(111). Solid: CV scanned up to -0.44 V. Dashed: waited at -0.44 V half an hour. Sweep rates: 2 mV/s.

### 5.3.3 Bulk Deposition

In this part, we investigated the adsorption behavior of copper in the bulk potential region after forming an adlayer in UPD region. The routine was as following: firstly scanning to -0.440 V, waiting at this potential half an hour, afterwards scanning further to more negative potentials (-0.575 V and -0.625 V).

The CVs illustrated at Fig 5.19.a indicate that scanning further to bulk potential region after obtaining monolayer of copper does not significantly accelerate the deposition of copper. Bulk deposition is still kinetically hindered.

The transients obtained from the same routine are also similar to transients drawn above (Fig 5.19.b). The areas under the transients are  $325 \pm 5 \mu\text{Ccm}^{-2}$  and  $351 \pm 5 \mu\text{Ccm}^{-2}$ . These values are not markedly larger than the value ( $305 \pm 5 \mu\text{Ccm}^{-2}$ , Fig. 5.16) obtained after just waiting at -0.440 V.

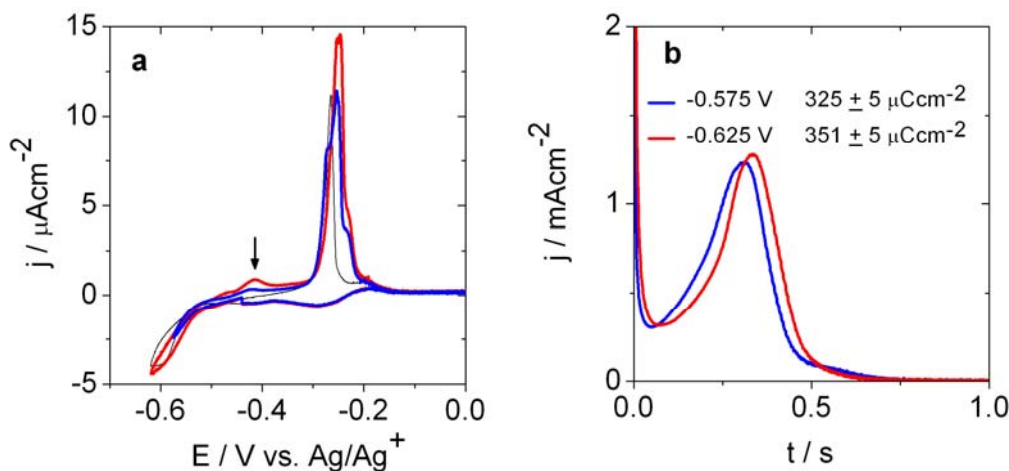


**Figure 5.19:** **a)** The cyclic voltammograms of 1 mM  $\text{CuClO}_4$ , 0.1 M  $\text{HClO}_4$  + 0.060 M  $\text{NaClO}_4$  on Au(111). Black: normal CV (without waiting). Red: on the anodic scan waited at -0.440 V half an hour, afterwards scanned further to -0.625 V. Blue: on the anodic scan waited at -0.440 V half an hour, afterwards scanned further to -0.575 V. Sweep rates: 2 mV/s. **b)** Current transients obtained from jumping from the end potentials to -0.15 V after waiting half an hour at -0.440 V (the colors correspond to the identical routine stated at a).

### 5.3.4 Ex situ XPS Studies

XPS measurements have been performed to analyze the chemical state of deposited copper atoms on the Au(111) surface at different emersion potentials. We prepared samples in 0.1 M  $\text{HClO}_4$ , 0.06 M  $\text{NaClO}_4$  and 1 mM  $\text{Cu}(\text{ClO}_4)_2$ . The potential of emersion is equal to the waiting potential. After removing the sample under potential control, we rinsed it with distilled water and dried under nitrogen stream. Afterwards, the samples were transferred to the vacuum chamber.

Fig. 5.20 shows the XPS survey spectra of copper deposited Au(111) samples prepared the following routines:

- I:* emersed after waiting 10 minutes at -0.55 V representing the deposition at bulk potential region.
- II:* emersed after waiting 30 minutes at -0.48 V representing the deposition at low underpotential.
- III:* emersed after waiting 30 minutes at -0.33 V representing the deposition at high underpotential.

All spectra were normalized according to the Au-4f peaks having a fixed area.

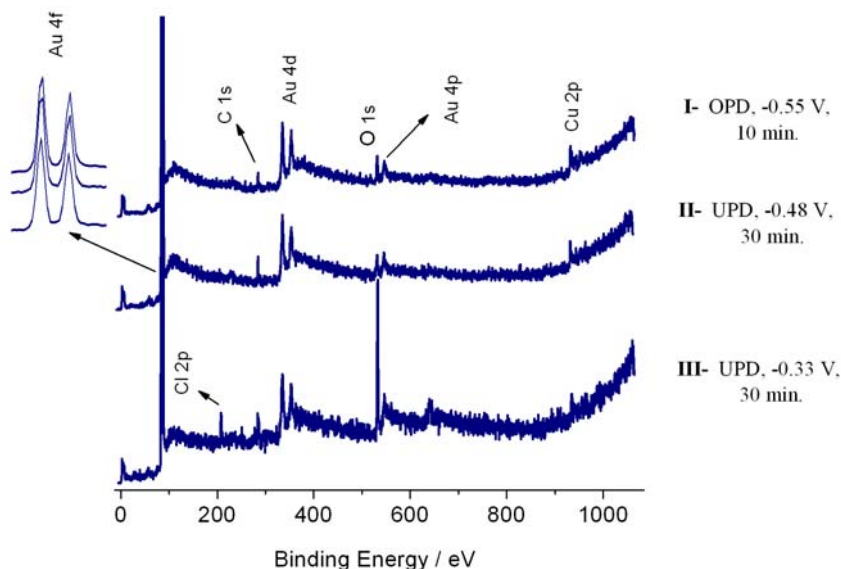


**Figure 5.20:** XPS survey spectra of copper deposited on Au(111) waiting and emersing at different potentials.

The survey spectra of I and II do not exhibit significant differences. However, the appearance of the Cl-2p peak (207.6 eV, formally  $\text{Cl}^{7+}$ ) and pronounced O-1s peak (532.4 eV) in the spectrum III implies the existence of perchlorate ( $\text{ClO}_4$ ) together with copper adatoms at the surface. Additionally, the ratio of the intensities of O-1s to Cl-2p is close to 4 considering the corresponding sensitivity factors. All C-1s signals are located at the same binding energy of 284.4 eV showing the contamination of the sample outside and inside of the UHV chamber.

### Cu-2p

The typical Cu-2p core level spectra taken from different copper deposited samples are shown in Fig 5.21. The common feature of all spectra is satellite peaks ( $\sim 944$  eV and  $\sim 963$  eV) which are located at higher binding energies than parent photoelectron lines. The strong satellite peaks are connected with shake-up transitions in  $\text{Cu}^{2+}$  compounds. These satellite peaks are of indicative of oxidized copper layer formation.

Secondly, the well separated multiple peaks at  $2p_{3/2}$  and  $2p_{1/2}$  binding energies of electrodeposited Cu are observed at the spectra I and II, whereas, the corresponding peaks at the spectrum III are not observed.

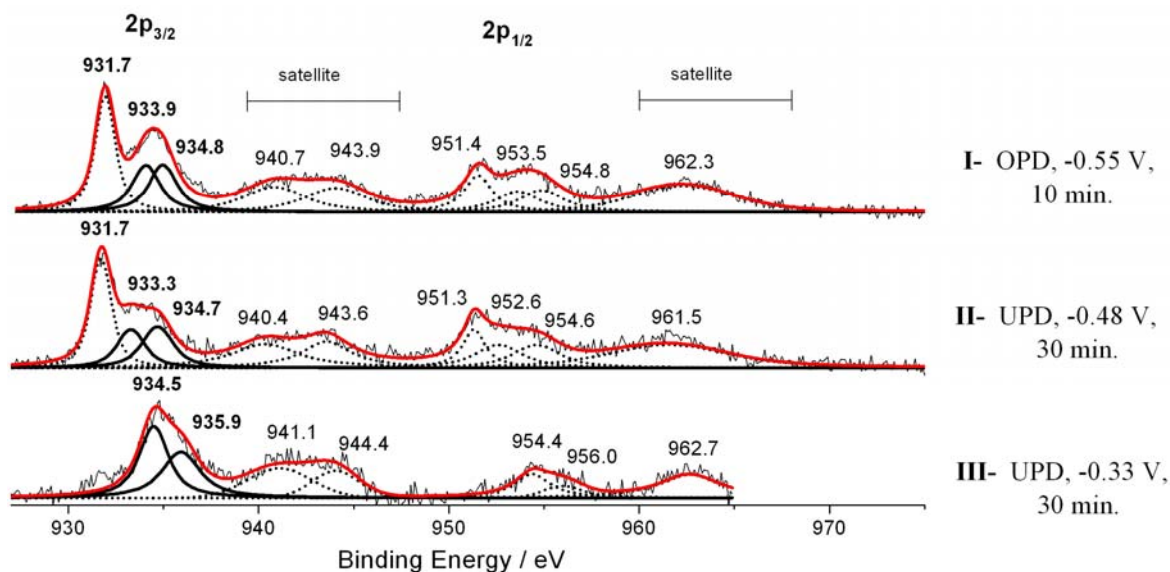


**Figure 5.21:** XPS Cu-2p spectra of copper deposited Au(111) by waiting and emersing at different potentials.

### **Spectra I and II**

It can firstly be stated that there is no significant difference between the spectra of the OPD (I) and the UPD (II). Analogous to the voltammetry results, this also indicates that the copper deposition in the OPD region is kinetically hindered.

The multiple signals at  $2p_{3/2}$  and  $2p_{1/2}$  core levels of I and II spectra tell us that the copper adatoms are present at two different chemical states. The signals are discussed separately as follows.

### **931.7 eV signals**

The signals located at 931.7 eV binding energies are about 0.7 eV lower than the corresponding value for bulk copper given in the literature <sup>[44, 153-156]</sup>. Similarly, Hammond and Winograd <sup>[44]</sup> have reported a 0.95 eV downshift of the UPD Cu vs. elemental Cu binding energy on Pt substrate forming more metallic deposit.

The reason of the lower binding energy may be a partial inter-diffusion of gold and copper atoms (partial alloy formation). Cu/Au alloys on Ru(100) have been investigated <sup>[154]</sup> and it has been shown that the  $2p_{3/2}$  signal of copper in alloys (Au/Cu 3:1) is downshifted by 0.4 eV. In general, the alloying of Cu and Au reduces the binding energy of the Cu-2p levels and increases



the binding energy of the Au-4f levels (as compared to the pure elements). XANES experiments indicate that these shifts are in part a consequence of an increase in Cu-3d electron population, and a reduction in the Au-5d electron population and the charge transfer is sensitive to the number of nearest neighbors of unlike atoms<sup>[155, 156]</sup>.

In the same line, Ruban et.al.<sup>[157]</sup> developed a model to explain the overall trends of the shifts in d-band positions due to the surface alloying or overlayer formation. They claim that if a “small” metal atom is moved into the lattice of a “larger” one, the neighbours are further away and the d-band width at the atom becomes smaller than at the surface of the elemental metal. This brings about an up-shift in the d-band center in order to maintain the same d-band filling locally. It leads to smaller binding energies in core bands behaving in the same manner.

From the other side, the formation of a Cu + Au alloy inevitably involves position exchange processes between Au and Cu atoms and would therefore generate a significant amount of surface imperfections upon anodic dissolution of copper. It is expected that such a process will manifest itself clearly in the highly sensitive current-potential traces. However, cycling of the potential in UPD region leaves the CV unchanged, suggesting that the topmost layer of Au atoms remains unperturbed by repeated deposition-dissolution of copper.

As conclusion, we can state that the negative shift in Cu-2p is a consequence of normal monolayer effect rather than an alloy formation. The copper adatoms are in metallic state.

### **~934.4 eV signals**

The signals around ~934.4 eV of all three spectra have a large FWHM (~3.0 eV). They can be fit with two components (each with ~1.5 eV FWHM) corresponding to two different oxidized ( $\text{Cu}^{n+}$ ,  $2 > n > 1$ ) adlayers. The case  $n=1$  is not possible due to the binding energy difference between Cu(0) and Cu(I) is  $< 0.2$  eV<sup>[158]</sup>. These two components might be the BE values of 933.7 eV for CuO and 934.4 eV for Cu(OH)<sub>2</sub>. If we want to find out the source of the copper oxide/hydroxide formation, we should remember the emersion procedure. After emersion, the probe was rinsed with water and then transferred to the vacuum chamber.

What happens during rinsing with water after emersion of the probe? For the answer Pourbaix diagram (potential vs. pH) of copper (Fig. 5.22) helps us to see the probable formation of Cu(OH)<sub>2</sub>, CuO and Cu<sub>2</sub>O. The main question to use the Pourbaix diagram is to know the

potential during the rinsing and the transfer. Will it be the emersion potential or not? According to Kolb, electrochemical double layer is frozen after emersion [105]. Therefore, mostly  $\text{Cu}_2\text{O}$  is formed if we consider this idea. However, there is not a strong evidence about the presence of Cu(I) signal in our XPS spectra. Secondly, it is experimentally investigated that copper is spontaneously oxidized at open circuit potential with water as the consequence of dissociative adsorption [159]. It leads to the formation of  $\text{Cu}(\text{OH})_2$ . From the free enthalpy values we know that the hydroxide  $\text{Cu}(\text{OH})_2$  is less stable than the oxide  $\text{CuO}$  and tends to be converted into the oxide [160].

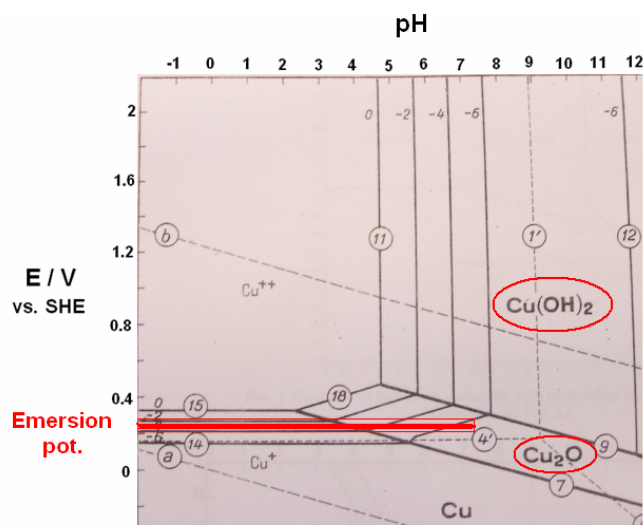


**Figure 5.22:** Pourbaix diagram of copper representing the metastable equilibrium [160].

Lastly, oxidation of copper might occur during the transferring of probe to the UHV chamber. It is well known that copper reacts rapidly with the oxygen from the air. Actually, we tried to avoid against the direct contact of air by introducing argon gas during transfer, but our instrumentation against oxidation was not so ideal. Therefore, most likely some part of oxidation took place during transfer. As a result, we can claim that  $\text{CuO}$  is most likely formed during rinsing and transfer.

### Spectrum III

The XPS data obtained after underpotential deposition of copper (at  $-0.33$  V) are very different from that obtained from which have been generated at  $-0.55$  V and  $-0.48$  V. The  $2p_{3/2}$  and  $2p_{1/2}$  signals of copper exhibit an upshift by  $3.1$  eV to  $934.9$  eV. In addition, one obtains a  $2p$  signal of Cl of perchlorate anion at  $207.6$  eV and a  $1s$  signal of oxygen at  $532.4$  eV. This result in

connection with the very low charge value ( $82 \mu\text{Ccm}^{-2}$ , section 5.3.2) during the dissolution process of the “UPD-layer” makes the interpretation difficult. On the other hand, the Avrami analysis of the dissolution transients (see Section 5.2.3.a) gives some hints about the formation a more ordered and stable adlayer as a possible result of perchlorate coadsorption.

The following model (Fig. 5.23) of the surface structure fulfills the requirements of the experimental results. We assume that an adlayer of  $\text{Cu}^{n+}$  ( $1 < n < 2$ ) is formed on top of the gold with the low coverage ( $\sim 0.33$ ). Two oxygen atoms of the perchlorate ions contact with the  $\text{Cu}^{n+}$  ion. In this layer water molecules may be incorporated.

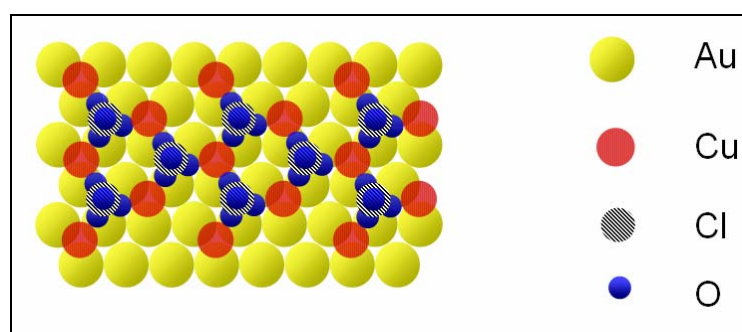


**Figure 5.23:** Schematic representation of copper UPD obtained upon waiting at high underpotential.

#### 5.4 Summary

- i) Copper deposition on Au(111) in the presence of sulphate anion proceeds faster and than that in the presence of perchlorate in the solution.
- ii) After the first step of Cu-UPD in the presence of sulphate anion, a honeycomb structure is formed. The oxidation state of copper adatoms is most likely between 0 and +0.5.
- iii) Both UPD and OPD of copper in perchloric acid solution are kinetically hindered. The formation of a full ML even at low underpotential takes place more than 20 minutes and the mechanism obeys the nucleation and growth law.
- iv) The dissolution transients of copper obtained from both sulphate and perchlorate containing electrolytes have well-defined minimum/maximum peaks. It indicates that dissolution process obeys “hole” nucleation and growth law.

- v) Deposition of copper at high underpotentials takes place very slowly. The expanded copper cations ( $\text{Cu}^{n+}$ ,  $1 < n < 2$ ) on Au(111) are incorporated with perchlorate anion.
- vi) At low underpotentials, perchlorate anion is not incorporated with copper adlayer. During UPD, Cu ions are almost fully discharged ( $\text{Cu}^{n+}$ ,  $n \sim 0$ ). However, after the emersion of sample outside two kinds of copper adatoms are observed; one is at metallic state, another is oxidized state. The oxidation of copper adlayer can take place during transfer (from air oxidation) and/or rinsing the probe with water.